Available online at www.sciencedirect.com

ScienceDirect

Solar Energy 129 (2016) 286–296

SOLAR ENERGY

www.elsevier.com/locate/solener

Effect of canopy profile on solar thermal chimney performance

P.J. Cottam [a,*], P. Duffour [a], P. Lindstrand [b], P. Fromme [c]

[a] Centre for Urban Sustainability & Resilience, Department of Civil, Environmental & Geomatic Engineering, University College London, Gower Street, London WC1E 6BT, United Kingdom

[b] Lindstrand Technologies Ltd, Maesbury Road, Oswestry, Shropshire SY10 8GA, United Kingdom

[c] Department of Mechanical Engineering, University College London, Gower Street, London WC1E 6BT, United Kingdom

Received 27 March 2015; received in revised form 17 January 2016; accepted 26 January 2016
Available online 19 February 2016

Communicated by: Associate Editor S.A. Sherif

Abstract

Solar thermal chimneys (STCs) are renewable energy power plants that require large-scale deployment to be economically competitive. This paper presents a steady-state analytical model developed to describe accurately the thermodynamics of the solar collector. The impact of different collector canopy designs on the performance is assessed. Results show that the height of the canopy has a significant effect on plant performance and that the canopy must be sufficiently high at the junction with the chimney to ensure maximum kinetic energy in the flow at the chimney inlet can be reached. A new collector profile with a partially sloped canopy is proposed. It was found to perform at similar levels of maximum power output to the best-performing existing canopy designs, and to be robust under varying environmental conditions. For ease of construction and reduction of associated costs this canopy can be built in stepped annular flat sections with only a minor loss in performance.

Keywords: Solar updraft tower; Solar collector; SCPP; SUPP

1. Introduction

The solar thermal chimney (STC) – also called a solar updraft tower – is a large scale solar power plant suited for desert deployment. It consists of a solar collector, which generates buoyant air; a tall chimney through which the buoyant air rises; and a turbine and generator set which extracts power from the pressure difference across it, generating electricity (Fig. 1a).

The largest STC prototype operated to date was constructed in Manzanares, Spain, in 1982, and was rated at 50 kW (Haaf et al., 1983). At the scales currently thought to be economically viable, power output can exceed 100 MW with a collector diameter larger than 5000 m and a chimney height of up to 1000 m (Pretorius and Kröger, 2006).

Different models for STC power plants have been proposed. Simple models assuming isobaric conditions within the collector were created by Zhou et al. (2007), who validated their model against a laboratory-scale physical prototype; by Gannon and von Backström (2000), who utilised an isobaric collector model within a thermodynamic cycle analysis; and by Cottam et al. (2012), who investigated the impact of plant dimensions on power output using a similar model.

Bernardes et al. (2003) and Pretorius and Kröger (2006) relaxed the assumption of isobaric conditions within the collector and developed more comprehensive analytical STC models. Both proposed steady-state models which

* Corresponding author.
E-mail address: p.cottam.11@ucl.ac.uk (P.J. Cottam).

http://dx.doi.org/10.1016/j.solener.2016.01.052
0038-092X/

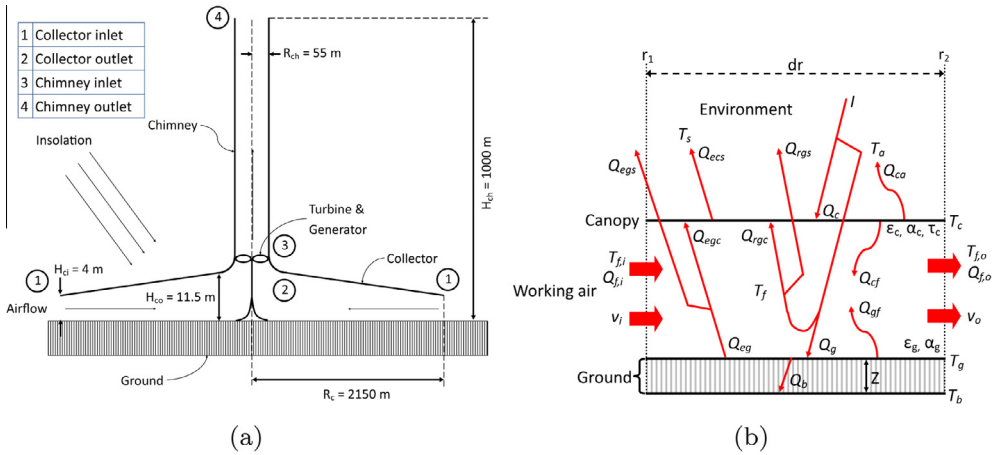

Fig. 1. (a) Schematic of the solar thermal chimney power plant with reference dimensions. (b) Energy flows between components and losses to ambient for a single discretised collector section.

calculate the air flow properties beneath the collector, with density calculated using the Boussinesq approximation (Bejan, 1993). Aware of the importance of collector thermodynamics in determining STC performance, these authors came together to compare the different methods of calculating heat transfer coefficients in their models (Bernardes et al., 2009). It was found that Pretorius and Kröger (2006) simulated both higher heat losses and heat gains than Bernardes et al. (2003), leading to similar predicted power output. More recently, Zhou et al. (2014) developed a steady state, compressible-flow model of the collector using a two-phase working fluid (humid air) to predict the performance of STC power plants in which the collector is affixed to a mountainside, reducing the required height of the chimney.

Studies using computational fluid dynamics (CFD) to simulate STCs include Fasel et al. (2013), in which the authors developed a 1:30 scale CFD model of the Manzanares STC prototype and compared it to a 1:250 scale experimental model constructed at their facilities. Sangi et al. (2011) derived a new pressure equation for STC air flow from Navier–Stokes and clarified discussions in the literature regarding the pressure profile in the collector, validating their findings against a CFD model incorporating ground heat storage. Ming et al. (2012) used CFD to assess the impact of ambient crosswind on STC performance.

Due to the novelty of the technology, STC construction and operation costs are difficult to forecast. Fluri et al. (2009), having identified some disparities in cost models published by Schlaich et al. (2004) and Bernardes (2004), proposed their own comprehensive cost model, coupled with a detailed analytical STC model. Comparing their physical and cost performance results to existing STC cost models, Fluri et al. (2009) predicted higher specific capital costs and lower power output for the same reference plant, resulting in a levelised electricity cost approximately three times higher than previously predicted. Thus, Fluri et al. (2009) have identified a clear need to reduce costs and increase performance further in order to bring STC power plants to market-ready status. Fluri et al. (2009) also calculated that the collector accounts for 74–83% of the total capital cost, meaning that cost-saving efforts should be focussed on the collector for greatest impact.

The role of collector canopy shape in reducing STC levelised electricity cost has received limited attention. In the eighteen papers presenting STC models surveyed in preparation for this article, nine utilised flat canopy profiles (Bernardes et al., 2003; Cottam et al., 2012; Fasel et al., 2013; Gholamalizadeh and Mansouri, 2013; Guo et al., 2013; Haaf et al., 1983; Koonsrisuk, 2012; Ming et al., 2012; Sangi et al., 2011); six utilised a constant-gradient canopy (von Backström, 2003; Dehghani and Mohammadi, 2014; Gannon and von Backström, 2000; Kasaeian et al., 2011; Pasumarthi and Sherif, 1998; Zhou et al., 2007); and three utilised a canopy profile in which the height rises exponentially from collector inlet to the central collector outlet (Fluri et al., 2009; Pretorius and Kröger, 2006, 2008). Bernardes (2010) investigated the effect of different canopy profiles on the air velocity and heat transfer in the collector. Pretorius and Kröger (2006, 2007) undertook brief studies of the role of the exponential canopy profile shape in determining power output, concluding that an exponential canopy designed such that it created a collector with constant cross-sectional flow area produced the greatest power output. Pasumarthi and Sherif (1998) studied the performance of a small-scale physical prototype STC with three different configurations of the collector, varying collector size and materials used. They concluded that introducing an intermediate absorber in the collector has the potential to boost mass flow rate.

Koonsrisuk and Chitsomboon (2013) studied the impact of canopy and chimney profile parameters by investigating flow area changes within the STC, with a view to increasing power output. They derived a theoretical expression showing how a collector canopy rising towards the chimney and a flaring chimney can boost power output by up to 400%,

validating their theoretical calculations with CFD analysis. Their model was limited to a constant heat transfer flux to the air over the collector area, and the turbine was not modelled. However, they provide compelling evidence that canopy designs other than the flat profile can lead to significant power gains. Beyond this, the impact of changing canopy profile types or parameters has not been studied in detail.

This contribution develops a theoretical STC model with a detailed thermodynamic analysis of the air flow and temperature rise under the collector, incorporating collector heat loss and surface shear stress. Different collector canopy profiles are systematically assessed, with a view to maximising power output whilst paying due consideration to engineering practicality.

2. Mathematical modelling

An analytical model of a solar thermal chimney power plant has been developed in order to compare systematically different collector canopy profiles. The main objective is to assess the maximum power output across a wide range of plant design parameters. Therefore a steady-state formulation was chosen as it is more efficient, with transient simulations mostly required when start-up and night-time operation need to be assessed.

The model presented here uses a similar approach to Bernardes et al. (2003) and Pretorius and Kröger (2006). It consists of a comprehensive thermo-fluids model for the collector and chimney. All flow within the collector is assumed to be axisymmetric and radial, reducing the collector to a one-dimensional flow problem with reducing circumferential area. The simulation problem is treated as steady state and the flow is assumed to be incompressible, using the Boussinesq approximation to capture the effect of change in fluid density. Turbine efficiency and the ratio of turbine pressure drop to chimney pressure drop are assumed to be fixed values and the working fluid is dry air (a single-phase gas). In order to reduce the number of variables which may impact upon system performance, the effects of ambient wind velocity across the top of the canopy surface, within the collector itself, and across the chimney outlet have not been investigated. They have previously been investigated in detail by Ming et al. (2012), Zhou et al. (2012) and Panse et al. (2011).

The model first simulates each STC component – the solar collector, the chimney and the turbine – separately. These component models are then coupled together to simulate the entire STC plant through an iterative process so that the input and output of each component converge to stable values. The steady-state model presented here was implemented in Matlab. It was designed to run rapidly in order to investigate systematically the influence of a wide range of key design parameters and environmental conditions. The reference parameters for the STC simulation are given in Table 1. These reference values were chosen for ease of comparison with existing models published in the literature (Fluri et al., 2009). A nomenclature is included in Table 2.

2.1. Collector

The collector is discretised along the radial path, forming linked annular discretised sections. The continuity equation is defined as

$$\frac{1}{r}+\frac{1}{\rho}\frac{\partial \rho}{\partial r}+\frac{1}{h_c}\frac{\partial h_c}{\partial r}+\frac{1}{v}\frac{\partial v}{\partial r}=0, \tag{1}$$

where r is the point on the collector radial path, measured from the collector centre; ρ is the air density; h_c is the height of the canopy at point r; and v is the mean air velocity at point r. Conservation of momentum is given by

$$\frac{\partial p}{\partial r}=\frac{-\tau}{h_c}-\rho v\frac{\partial v}{\partial r}, \tag{2}$$

where p is the air pressure at point r, and τ is the sum of the shear stresses due to the working fluid interaction with the ground surface (of roughness length e_{rg}) and the underside of the canopy (of roughness length e_{rc}). It is determined using

$$\tau=\frac{f_d}{8}\rho v^2, \tag{3}$$

where f_d is the dimensionless Darcy Friction Factor calculated as described in Pretorius and Kröger (2006). Changes in density are assumed to be a function of temperature only, such that the equation of state reduces to

$$\frac{\mathrm{d}\rho}{\mathrm{d}T}=\frac{\rho}{T}, \tag{4}$$

where T is the mean air temperature at the annulus of radius r. This is the Boussinesq approximation, and is valid only for small changes in density (Bejan, 1993).

The energy flows between collector components within a discretised collector section are shown diagrammatically in Fig. 1b and the associated energy balance equations are as follows:

Collector canopy:

$$IA\alpha_c+\dot{Q}_{egc}+\dot{Q}_{rgc}=\dot{Q}_{ecs}+\dot{Q}_{c\infty}+\dot{Q}_{cf}; \tag{5}$$

Working air:
The equation for the energy flow of the working air contains the kinetic energy term which accounts for the conversion of thermal into mechanical energy:

$$\dot{Q}_{cf}+\dot{Q}_{gf}=\dot{m}c_p\Delta T+\frac{\dot{m}}{2}\left(v_o^2-v_i^2\right); \tag{6}$$

Frictional shear stress constitutes a second order term, and hence is disregarded in the working air energy equation. However, it is included in the momentum conservation.

Ground surface:

$$IA\tau_c\alpha_g=\dot{Q}_{eg}+\dot{Q}_{gf}+\dot{Q}_b, \tag{7}$$

Table 1
Parameter values used in simulations. Reference values are used when other values are varied. The range across which parameters vary is given in the Range column.

Parameter	Reference value	Range
Collector		
R_c – Collector radius	2150 m	
H_{ci} – Canopy height at inlet	4 m	4–15 m
H_{co} – Canopy height at outlet	11.5 m	4–15 m
r_{grad} – Point of canopy gradient change along radial path	720 m	55–2150 m
α_c – Canopy absorptivity (glass)	0.30	
τ_c – Canopy transmissivity (glass)	0.70	
e_{rc} – Canopy roughness length	0.002 m	
Chimney		
R_{ch} – Chimney internal radius	55 m	
H_{ch} – Chimney height	1000 m	
e_{rch} – Chimney internal surface roughness length	0.002 m	
Turbine		
x – Ratio of turbine to chimney pressure drop	0.81	
η_t – Turbine & powerblock efficiency[a]	0.75	
Environmental		
Ground material	Sandstone	
ϵ_g – Ground emissivity[b]	0.90	
α_g – Ground absorptivity[b]	0.90	
ρ_{rg} – Ground reflectivity	0.10	
ρ_g – Ground material density[b]	2160 kg m^{-3}	
c_{pg} – Ground specific heat capacity[b]	710 J kg^{-1} K^{-1}	
k_g – Ground conductivity[b]	1.83 W m^{-1} K^{-1}	
e_{rg} – Ground surface roughness length	0.02 m	
z_b – Depth below ground at which $\frac{\partial T}{\partial z} = 0$	5 m	
T_b – Temperature at depth z_b	283 K	
T_∞ – Ambient air temperature (ground level)	305 K	
p_∞ – Ambient air pressure (ground level)	101,325 Pa	
c_p – Specific heat capacity of air	1008.5 J kg^{-1} K^{-1}	
μ – Air viscosity	1.85×10^{-5} Pa s	
RH – Relative humidity of air	0.20	
v_w – Ambient wind velocity	0 ms^{-1}	
I – Insolation	900 W m^{-2}	300–975 W m^{-2}

[a] Values obtained from Bernardes et al. (2003).
[b] Values obtained from Pretorius and Kröger (2006).

Subscript r denotes reflected radiation, subscript e denotes emitted radiation, subscripts g, f and c denote ground, working air and canopy properties respectively, subscripts b, s and ∞ denote heat loss to ground, sky (in the case of radiative heat transfer), and ambient environment (in the case of convective heat transfer) respectively, whilst subscripts i and o denote properties at the discretised section inlet and outlet respectively.

All $\dot{Q}$ terms in Eqs. (5)–(7) expand into one of the following forms. Convective energy flows expand into

$$\dot{Q} = hA\Delta T, \tag{8}$$

where h is the heat transfer coefficient; A is the plan-view area of the annular discretised section under consideration; and ΔT is the difference in temperature between the solid surface and the fluid. The heat transfer coefficients depend on the magnitude of the temperature difference between the surface and the fluid; whether the surface is heated or cooled; and whether it faces up or down (Bernardes et al., 2003; Pretorius and Kröger, 2006). Some oscillatory behaviour has been observed in the fluid temperature profiles across short lengths of the collector radial path due to the model switching between two different heat transfer equations.

Radiative energy flows expand into

$$\dot{Q}_r = h_r A \Delta T \tag{9}$$

where h_r is the radiative heat transfer coefficient calculated by the Stefan–Boltzmann Law for heat radiated from one body (subscript 1) and absorbed by a second body (subscript 2) divided by the temperature difference ΔT (Bernardes et al., 2003):

$$h_r = \frac{\sigma(T_1^2 + T_2^2)(T_1 + T_2)}{\frac{1}{\epsilon_1} + \frac{1}{\epsilon_2} - 1}, \tag{10}$$

where ϵ denotes emissivity.

Energy flow convected by working air flow through the collector is defined by

$$\dot{Q}_f = \dot{m} c_p \Delta T, \tag{11}$$

Table 2
Nomenclature. Defines terms not defined in Table 1.

Roman symbols	
r	Radial position (m)
h	Height position (m)
v	Velocity (ms^{-1})
p	Pressure (Pa)
f_d	Darcy friction factor
T	Temperature (K)
$\dot{Q}$	Heat flow (W)
c_p	Specific heat (constant pressure) ($J\,kg^{-1}\,K^{-1}$)
k	Conductivity ($W\,m^{-1}\,K^{-1}$)
z	Depth (m)
A	Area (m^2)
$\dot{m}$	Mass flow rate ($kg\,s^{-1}$)
R	Specific gas constant of air = 287.05 $J\,kg^{-1}\,K^{-1}$
b	Canopy shape exponent
Greek symbols	
ρ	Density ($kg\,m^{-3}$)
η	Efficiency
ϵ	Emissivity
σ	Boltzmann constant = 5.67×10^{-8} $W\,m^{-2}\,K^{-4}$
Subscripts	
c	Collector or canopy
r	Reflected
e	Emitted
g	Ground
s	Sky
∞	Ambient air
f	Working fluid
t	Turbine
ch	Chimney
$grad$	Point of gradient change
b	Underground or buoyancy
i	At inlet
o	At outlet
$trans$	In the collector-to-chimney transition section
v	Available to generate velocity

where in this instance, ΔT represents the difference in working fluid temperature between the outlet and inlet.

Suitable phenomenological equations for dynamic convective heat transfer coefficients were obtained from Pretorius and Kröger (2006).

For each discretised collector section, Eqs. (1)–(7) are solved iteratively in two steps. In the first step, the fluid flow properties are found using discretised versions of mass continuity (Eq. (1)), conservation of momentum (Eqs. (2) and (3)) and the Boussinesq approximation (Eq. (4)). In the second step, the energy balance equations (Eqs. (5)–(7)) are solved for the component temperatures. In this step, radiative heat transfer terms are linearised with respect to temperature and the kinetic energy term in Eq. (6) is calculated using values of the velocity found in step 1. Steps 1 and 2 are repeated until the component temperatures, the flow velocity, pressure and density have converged to values that satisfy all seven equations.

2.2. Collector-to-chimney transition section

In most STC designs, the heated working air exiting the collector at the collector centre transitions from radial to axial flow by means of a large conical structure which guides the airflow towards the chimney inlet. It is assumed that all solid surfaces enclosing the flow in the transition section are adiabatic and the flow itself is isothermal. The flow problem is thus reduced to the Bernoulli equation:

$$\Delta p_{trans} = \frac{1}{2}\rho_{co} v_{co}^2 \left(1 - \left(\frac{A_{co}}{A_{chi}}\right)^2\right), \tag{12}$$

where $\Delta p_{trans} = p_{co} - p_{chi}$; subscript *co* denotes properties at the collector outlet; and subscript *chi* denotes properties at the chimney inlet.

2.3. Chimney and turbines

It is assumed that the air rising through the chimney is undergoing a process of isentropic expansion and that the chimney walls are adiabatic (Bernardes et al., 2003; Pretorius and Kröger, 2006). Using values for a proposed concrete chimney design (Harte et al., 2012), the heat loss through the chimney wall was estimated at less than 1%, justifying the adiabatic assumption. Density, as a function of height, is thus expressed as

$$\rho(h) = \rho(0)\left(1 + \frac{(\kappa - 1)gh}{\kappa R T_0}\right)^{\frac{1}{\kappa - 1}}, \tag{13}$$

where $\kappa = 1.235$ for ambient air and $\kappa = 1.4005$ for working air (Bernardes et al., 2003); h is the height of the parcel of air under scrutiny; and T_0 is the temperature of the air at $h = 0$. The density terms are used to calculate the chimney pressure difference driving the flow at height $0 \leqslant h \leqslant H_{ch}$, as

$$\Delta p_b = \int_h^{H_{ch}} g(\rho_\infty - \rho_{ch})\mathrm{d}h \tag{14}$$

Δp_b represents the total pressure difference generated by air flow buoyancy. It is attenuated by a pressure drop due to friction Δp_f. Constant characteristics of the turbine and power block have been assumed for simplicity. More elaborate models can be developed by consulting the literature, e.g. Korpela (2011). The ratio of turbine pressure drop to total chimney pressure difference is fixed at $x = 0.81$, identified as optimum by Bernardes and Zhou (2013) and corroborated by the model presented herein (results not shown), such that

$$\Delta p_t = x(\Delta p_b - \Delta p_f). \tag{15}$$

The pressure loss due to friction is expressed as

$$\Delta p_f = \frac{1}{2}\rho_{chi} f_d \frac{H_{ch}}{2R_{ch}} v_{chi}^2, \tag{16}$$

in which f_d is the Darcy Friction Factor, determined following Pretorius and Kröger (2006).

The pressure difference available to generate velocity is therefore

$$\Delta p_v = (1 - x)(\Delta p_b - \Delta p_f). \tag{17}$$

The mass flow rate generated by the chimney is defined as

$$\dot{m} = \pi R_{ch}^2 \sqrt{2\rho \Delta p_v}, \tag{18}$$

with all values taken at the chimney inlet.

Assuming a constant turbine and generator efficiency of $\eta_t = 0.75$, the turbine pressure difference drives the power output P such that

$$P = \eta_t \frac{\dot{m}}{\rho} \Delta p_t. \tag{19}$$

Cold inflow at the chimney outlet – a particular risk during start-up or low-insolation periods – is not considered as the model is simulating the STC at peak insolation. Pretorius and Kröger (2008) assessed a range of plant configurations to find those very large STCs susceptible to cold inflow, and from their data it can be inferred that for the proposed dimensions of the plant considered in this paper, cold inflows are not to be expected.

2.4. Model validity checks

The STC model described herein has been found to satisfy continuity and conservation of momentum, and has been tested for a wide range of environmental conditions and plant dimensions. The use of the Boussinesq approximation was found to lead to a difference compared to the Ideal Gas behaviour of five orders of magnitude less than the temperature rise itself, and thus is justified. The energy balance for the complete collector was satisfied with a relative error of less than 0.1%, and the energy balance for the airflow was found to be accurate to less than 0.001%.

Bernardes et al. (2009) assessed two comprehensive models in the STC literature, that of Pretorius and Kröger (2006), and that of Bernardes et al. (2003). Minor differences between their models produced variation in their power output of up to 15%. The same data points simulated with the model presented in this paper yielded a difference of no greater than 13%, confirming that this model simulates the STC accurately.

For a plant of the same reference dimensions as those used in this paper, Schlaich et al. (2004) predicted a power output of 100 MW and Fluri et al. (2009) predicted a power output of 66 MW. The model presented herein predicts a power output of 74 MW. In the absence of defined environmental parameters from Fluri et al. (2009) – the authors were conducting a study of power output over a year – it was assumed that insolation $I = 900\ \mathrm{W\,m^{-2}}$ and ambient temperature $T_\infty = 305\ \mathrm{K}$, representative of a desert environment.

Performance data from the Manzanares STC prototype was extracted from Haaf (1984), along with available data on ambient temperature and material properties. For this data the simulated power output ranged from 27 kW to 35 kW, across a range of insolation values from $830\ \mathrm{W\,m^{-2}}$ to $910\ \mathrm{W\,m^{-2}}$ and ambient temperature from 297 K to 309 K. This was 3–9% less than the recorded power outputs from the Manzanares prototype, demonstrating that the model presented herein delivers an accurate but conservative estimate of power output.

3. Investigation into canopy profile design

This section assesses the performance of the three canopy profile types employed in literature (flat, constant-gradient sloped, and exponential) as well as two proposed new profile types (segmented and stepped). These profiles are shown diagrammatically in Fig. 2. Their suitability in terms of power output and engineering practicality (i.e. ease of construction and maintenance) are investigated and performance comparison is based on results shown in Figs. 3–5. Fig. 3 shows the power output for each profile when key design parameters are varied. Fig. 4 shows how the flow properties change as the working air flows under each canopy profile. Fig. 5 shows the working air mean velocity and pressure difference between ambient and working air at the chimney inlet for the different canopy profiles, as the product of these two quantities is a good indication of the plant power output (Eq. (19)).

The following sub-sections assess each canopy profile in turn to find the best-performing design for each type. Results are shown for the reference plant dimensions specified in Table 1, unless otherwise stated.

3.1. Exponential canopy profile

The exponential canopy shape is defined by

$$h_c(r) = H_{ci} \left(\frac{R_c}{r} \right)^b, \tag{20}$$

where $h_c(r)$ is the canopy height at point r on the collector radial path (r decreases from R_c towards zero at the centre of the collector); H_{ci} is the canopy height at the collector inlet; R_c is the collector radius; and b is the canopy profile exponent which defines the shape of the canopy (Fig. 2a).

Fig. 3a shows that the exponential canopy with $b = 0.42$ for an inlet height $H_{ci} = 4$ m generates a maximum highest power output of 74 MW, with a canopy outlet height of 19 m. The plots shown in Fig. 4 detail the main flow properties of the fluid along the radial path under the collector from right (inlet) to left (chimney). The overall behaviour is broadly similar for all canopy types: the working air temperature increases by approximately 20 K within the collector, as shown in Fig. 4a. The temperature plateaus along the radial path as the collector components tend towards thermal equilibrium. Following the Boussinesq approximation (Eq. (4)), this temperature rise results in a density drop which drives the buoyancy flow up the chimney. Fig. 4b shows the increase in air velocity and Fig. 4c a small decrease in static pressure close to the chimney due to the decreasing flow cross section. Setting exponent $b = 1$ would create a constant flow cross section throughout the collector and would result in an almost constant air velocity and pressure as the flow would not be constricted.

However, it should be noted that altering the value of exponent b changes the collector outlet height, thereby altering the geometry of the collector-to-chimney transition section (see Fig. 3a). Eq. (12) shows that the ratio of flow cross section areas at the collector-to-chimney transition determines the pressure drop through this section. For this reason, it is important to consider flow properties at the chimney inlet, as well as through the collector.

From Fig. 5a, it can be seen that initially both the pressure drop and the air velocity at the chimney inlet increase with the exponent b, but that both decrease for higher values of b, leading to lower power outputs (Fig. 3a). Furthermore, a collector inlet height of 4 m and a canopy exponent of $b = 1$ would lead to an outlet height of 156 m for the reference STC plant dimensions. Such a large canopy outlet height, coupled with the complex canopy shape, would make design, manufacture and maintenance of the collector prohibitively expensive.

3.2. Flat canopy profile

The flat canopy has the same height throughout the collector (Fig. 2b), and has the advantage of being simple and relatively cheap to construct and maintain (for moderate heights at least). Due to its simplicity, it has been used for many physical prototypes, not least the Manzanares STC plant (Haaf et al., 1983). Varying the canopy height, it was found that STC performance peaks at $H_c = 9$ m and $P = 63$ MW, or 85% of the best-performing exponential canopy (Fig. 3b). Such a height is tall enough to make construction and maintenance difficult. However, Fig. 3b shows that a lower flat collector imposes a severe performance penalty (23% power loss for $H_c = 4$ m), resulting in the low pressure difference and low air velocity at the chimney inlet seen in Fig. 5b. The air velocity along the collector radial path increases significantly due to the decreasing flow cross section (Fig. 4b), reaching the point where air compressibility may no longer be negligible. As the velocity rises, the static pressure drops close to the chimney (Fig. 4c). For outlet canopy heights beyond 9 m, the power output falls slightly due to the change of ratio of collector outlet flow area to chimney inlet flow area, which results in a reduction in chimney inlet air velocity (Fig. 5b).

3.3. Constant-gradient sloped canopy profile

For the constant-gradient profile, the canopy height increases linearly from the collector inlet height H_{ci} at the periphery to the collector outlet height H_{co} at the collector centre (Fig. 2c). Depending on the gradient, this can result in an increasing flow area for parts of the collector and an associated decrease of the air velocity. This "bathtub" effect, identified by Bernardes (2010), leads to lower heat transfer coefficients and thus lower collector efficiency. For the reference STC with a canopy inlet height of 4 m, the best-performing configuration has a canopy outlet height of 11.5 m, generating 69 MW, a 7% performance drop compared to the best-performing exponential canopy (Fig. 3). The temperature rise, air velocity, and pressure for the sloped canopy profile mostly lie between those of the exponential and flat profiles in line with the collector height (Fig. 4). System performance is robust for taller output canopies, i.e. larger canopy outlet heights only cause a small reduction in power output due to the reduction of chimney air velocity (Fig. 5c). Additional simulations (results not shown) confirmed that the best performing sloped canopy profile does not change with varying insolation or ambient temperature, so that the same profile can be recommended for most environmental conditions. All other simulation parameters are as specified in Table 1.

3.4. Segmented canopy profile

The rationale behind this canopy profile was to develop a profile shape delivering the performance benefits of the exponential canopy whilst limiting the additional cost due

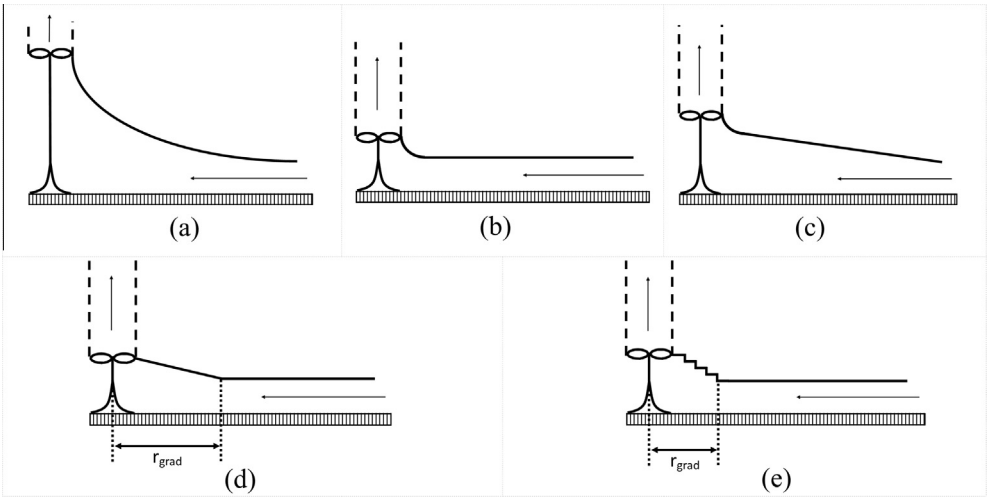

Fig. 2. STC collector canopy profiles: (a) exponential; (b) flat; (c) constant-gradient sloped; (d) segmented; and (e) segmented & stepped.

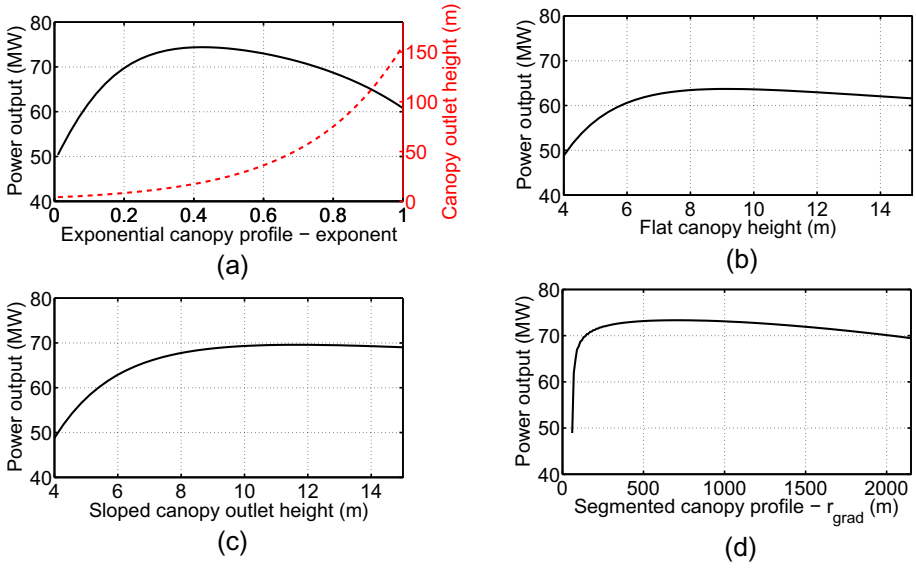

Fig. 3. Power output for different canopy profiles: (a) exponential; (b) flat; (c) constant-gradient sloped; and (d) segmented; (reference STC, $H_{ci} = 4$ m, $I = 900$ Wm^{-2}, $T_\infty = 305$ K).

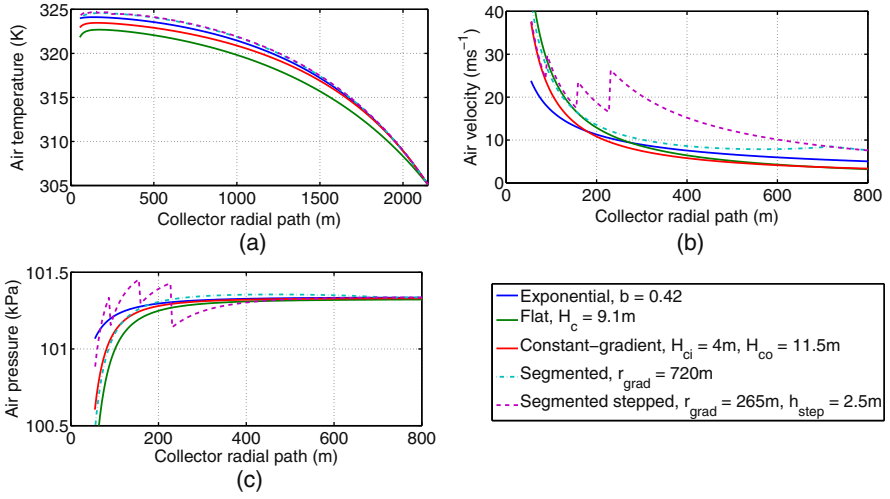

Fig. 4. Collector air flow properties: (a) mean air temperature; (b) mean air velocity; and (c) mean air pressure along the radial path (reference STC, $I = 900$ W m^{-2}, $T_\infty = 305$ K).

to increased construction complexity. The segmented canopy profile is flat at the outer periphery, rising linearly from radial point r_{grad} up to the chimney (Fig. 2d). The effect of changing the location of r_{grad} has been investigated, keeping the inlet height and the outlet height as those of the best performing constant-gradient profile ($H_{ci} = 4$ m, $H_{co} = 11.5$ m).

The best-performing configuration ($r_{grad} = 720$ m) generates 73 MW (Fig. 3d), 4% higher than the constant-gradient profile and almost equal to the best-performing exponential collector, without the same canopy height requirements at the chimney outlet. In order to investigate the robustness of the optimum configuration, the power output was calculated for varying environmental conditions. Power output increases with increasing insolation, and the value of r_{grad} giving a maximum power output changes only slightly, except at very low insolation (Fig. 6). Similar results (not shown) confirmed that the value of r_{grad} yielding optimum power output is not sensitive to ambient temperature (tested range: 296–314 K). Setting r_{grad} too close to the collector outlet imposes losses as it restricts the flow. For the best-performing configuration ($r_{grad} = 720$ m) 11% of the collector area will require construction with increased canopy height. The air velocity (and thus mass flow rate) at the chimney for this configuration approximately matches that of the constant-gradient and exponential canopies, but the pressure drop is slightly lower (Fig. 5d). Fig. 4b shows the increased air velocity under the flat part of the canopy (to 720 m), which then gradually approaches the constant-gradient case. This

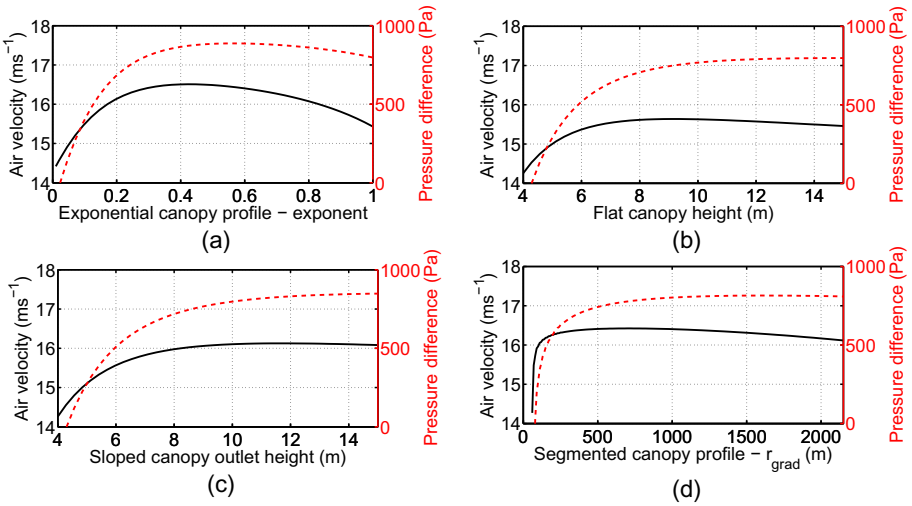

Fig. 5. Working air mean velocity and pressure difference between ambient and working air at chimney inlet for different collector canopy profile types and dimensions. Reference STC dimensions and environmental conditions. $H_{ci} = 4$ m unless otherwise specified.

leads to a small pressure increase due to the change in canopy profile (Fig. 4c), which is partially balanced by the slightly higher air temperature rise (Fig. 4a).

By keeping the collector height low for the majority of the flow path, the segmented collector canopy ensures that higher air velocities are maintained within the collector (Fig. 4b), inducing higher rates of convective heat transfer from the upper and lower surfaces. The reduction in air velocity for linearly sloped canopies identified by Bernardes (2010) is not observed in Fig. 4 as the chosen configurations of each canopy design are the best-performing of their type and hence do not exhibit this behaviour.

One of the aims of this investigation is to provide cost-effective performance enhancements by modifying the canopy design. A canopy with $r_{grad} = 265$ m is proposed as a compromise between construction costs and power output, for which only 1.5% of the collector area has a gradient. This will provide a power output of 72 MW, only a 2% performance loss compared to the best-performing exponential canopy, and less than a 1% loss compared to the best-performing segmented canopy.

3.5. Stepped canopy profile

Practical engineering considerations suggest that non-flat canopy profiles discussed in this paper would most likely be constructed as a series of horizontal annular canopy sections joined by short transition sections (Fig. 2e). To investigate such a design, the sloping region of the segmented profile was approximated by steps of different heights such that the volume under the canopy remained approximately the same. The transition between these steps is modelled as a vertical increase in height, but would in all likelihood be constructed as a short sloping region to reduce recirculation losses.

A segmented, stepped canopy profile with $H_{ci} = 4$ m, $r_{grad} = 265$ m and $h_{step} = 2.5$ m (i.e. consisting of three equal-height steps from $h_c = 4$–6.5 m at $r_c = 265$ m; from $h_c = 6.5$–9 m at $r_c = 195$ m; and from $h_c = 9$–11.5 m at $r_c = 125$ m), generates 71 MW power output, only 5% less than the best-performing case and only 2% less than the same segmented profile without the steps. Fig. 4b shows that the air velocity curve follows that of the segmented profile with jumps associated with each step in the collector height. Fig. 4 c shows the matching behaviour in the pressure profiles due to the canopy height jumps with a slightly higher pressure at the collector outlet responsible for the marginal reduction in output power. Therefore the stepped profile offers the same performance advantages as the segmented profile - that of maintaining a low canopy height for the majority of the collector radial path to boost air velocity and thus heat transfer - but with much lower construction complexity.

3.6. Overall comparison

Comparison between Figs. 3 and 5 reveals some important features. The canopy must have sufficient height to obtain higher power output – this is especially true of the collector outlet height. Once a certain height threshold has been reached, power output is less sensitive to canopy height or the actual canopy shape. This means that engineering practicality can take precedence and simpler collector designs can be chosen, such as the segmented stepped canopy that generates similar power output at lower construction cost. For canopies with sufficient height, the plant power output curves in Fig. 3 follow closely the chimney inlet velocity shown in Fig. 5. This means that the collector to chimney transition is important and that the mass flow rate is the key driver for increased power generation.

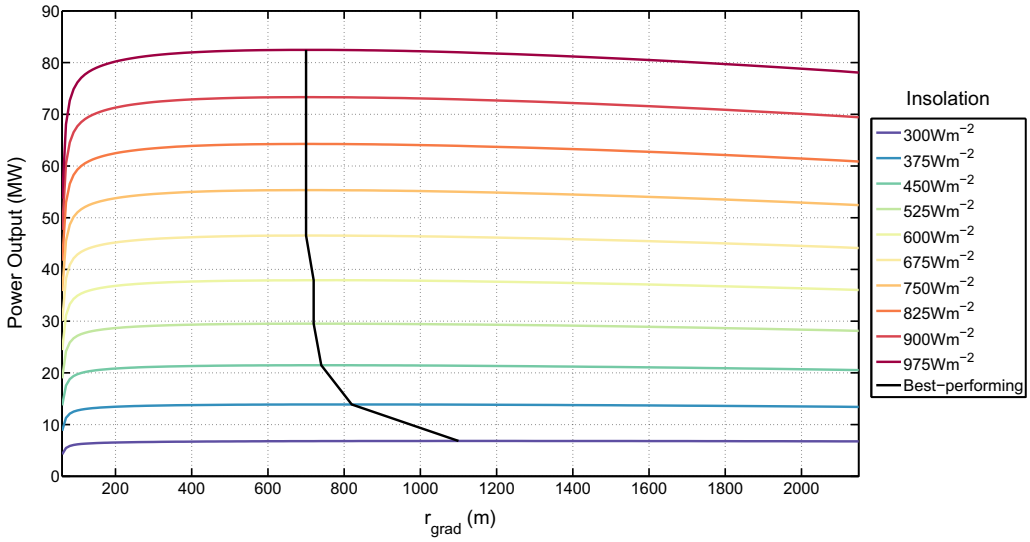

Fig. 6. STC performance for varying values of r_{grad} under different levels of insolation. $T_\infty = 305$ K, $R_c = 2150$ m, $H_{ch} = 1000$ m, $H_{ci} = 4$ m, $H_{co} = 11.5$ m.

4. Conclusions

In order to advance STC technology towards commercial deployment the economic viability needs to be improved. This study investigated whether improved canopy designs could reduce cost at little-to-no loss in power generation. An efficient analytical, steady-state simulation model of the STC power plant has been developed, with a detailed model of the collector including coupling of the heat transfer and fluid dynamics along the collector radial path. The model was used to investigate the peak power output for various system dimensions and collector canopy profiles. The results shown indicate that the design of the canopy influences the plant power performance in a significant but non-straightforward way.

Existing literature has focussed mainly on canopy profiles which are either flat, sloped at a constant gradient, or exponential. Flat canopies are simple to design, but cause pressure losses due to the restriction of the air flow cross section, especially close to the chimney. A constant-gradient sloped canopy can improve power output. The exponential canopy profile allows performance improvements, but construction and maintenance could be difficult and costly due to access issues. For the best-performing design of each canopy profile, the temperature rise and associated density drop under the collector were found to be quite similar. The canopy outlet height was shown to be an important parameter as it defines the pressure drop in the flow through the collector-to-chimney transition section. This highlighted the importance of sufficiently increasing the cross-sectional flow area near the chimney to prevent pressure losses.

This study proposes instead a segmented canopy profile which is flat from the collector periphery to a point r_{grad} on the radial path, from which the canopy height increases with a constant gradient or in flat steps. The segmented canopy profile almost matches the power output of the best-performing exponential profile and uses a simpler design, reducing both construction and maintenance costs. The stepped, segmented canopy profile is likely to provide a good compromise between power output to construction cost. The predicted power generation for such a segmented canopy design was found to be highly robust for a wide range of environmental conditions. Further work will be required to quantify the potential cost savings and to investigate additional factors which influence the predicted power generation, such as ambient wind, frictional and heat losses.

Acknowledgements

The authors are grateful to Lindstrand Technologies Ltd, the UK Engineering & Physical Sciences Research Council (EPSRC), the Centre for Urban Sustainability & Resilience at University College London (UCL), and the Royal Commission for the Exhibition of 1851 for their continued support of this research.

References

Bejan, A., 1993. Heat Transfer. John Wiley & Sons.

Bernardes, M.A.d.S., 2004. Technische, ökonomische und ökologische Analyse von Aufwind-kraftwerken, Ph.D. thesis. Universität Stuttgart.

Bernardes, M.A.d.S., 2010. Solar chimney power plants developments and advancements. In: Solar Energy, pp. 171–186.

Bernardes, M.A.d.S., Zhou, X., 2013. Strategies for solar updraft tower power plants control subject to adverse solar radiance conditions. Solar Energy 98, 6–13.

Bernardes, M.A.d.S., Voß, A., Weinrebe, G., 2003. Thermal and technical analyses of solar chimneys. Solar Energy 75, 511–524.

Bernardes, M.A.d.S., von Backström, T., Kröger, D., 2009. Analysis of some available heat transfer coefficients applicable to solar chimney power plant collectors. Solar Energy 83, 264–275.

Cottam, P., Duffour, P., Fromme, P., 2012. A parametric study of solar thermal chimney performance. In: Proceedings of the ISES EuroSun Conference 2012.

Dehghani, S., Mohammadi, A.H., 2014. Optimum dimension of geometric parameters of solar chimney power plants – a multi-objective optimization approach. Solar Energy 105, 603–612.

Fasel, H.F., Meng, F., Shams, E., Gross, A., 2013. CFD analysis for solar chimney power plants. Solar Energy 98, 12–22.

Fluri, T.P., Pretorius, J.P., Van Dyk, C., Von Backström, T.W., Kröger, D.G., Van Zijl, G.P.A.G., 2009. Cost analysis of solar chimney power plants. Solar Energy 83, 246–256.

Gannon, A.J., von Backström, T.W., 2000. Solar chimney cycle analysis with system loss and solar collector performance. J. Solar Energy Eng. 122, 133–137.

Gholamalizadeh, E., Mansouri, S., 2013. A comprehensive approach to design and improve a solar chimney power plant: a special case – Kerman project. Appl. Energy 102, 975–982.

Guo, P., Li, J., Wang, Y., Liu, Y., 2013. Numerical analysis of the optimal turbine pressure drop ratio in a solar chimney power plant. Solar Energy 98, 42–48.

Haaf, W., 1984. Solar chimneys part II: preliminary test results from the Manzanares pilot plant. Int. J. Solar Energy 2, 141–161.

Haaf, W., Friedrich, K., Mayr, G., Schlaich, J., 1983. Solar chimneys part I: principle and construction of the pilot plant in Manzanares. Int. J. Solar Energy 2, 3–20.

Harte, R., Graffmann, M., Krätzig, W.B., 2012. Optimisation of solar updraft chimneys by nonlinear response analysis. In: Proceedings of the International Conference on Solar Updraft Tower Power Technology, pp. 193–202.

Kasaeian, A., Heidari, E., Vatan, N., 2011. Experimental investigation of climatic effects on the efficiency of a solar chimney pilot power plant. Renew. Sustain. Energy Rev. 15, 5202–5206.

Koonsrisuk, A., 2012. Mathematical modeling of sloped solar chimney power plants. Energy 47, 582–589.

Koonsrisuk, A., Chitsomboon, T., 2013. Effects of flow area changes on the potential of solar chimney power plants. Energy 51, 400–406.

Korpela, S.A., 2011. Principles of Turbomachinery. John Wiley & Sons, Hoboken.

Ming, T., Wang, X., de Richter, R.K., Liu, W., Wu, T., Pan, Y., 2012. Numerical analysis on the influence of ambient crosswind on the performance of solar updraft power plant system. Renew. Sustain. Energy Rev. 16, 5567–5583.

Panse, S., Jadhav, A., Gudekar, A., Joshi, J., 2011. Inclined solar chimney for power production. Energy Convers. Manage. 52, 3096–3102.

Pasumarthi, N., Sherif, S.A., 1998. Experimental and theoretical performance of a demonstration solar chimney model – part I: mathematical model development. Int. J. Energy Res. 22, 277–288.

Pretorius, J.P., Kröger, D.G., 2006. Solar chimney power plant performance. J. Solar Energy Eng. 128, 302–311.

Pretorius, J.P., Kröger, D.G., 2007. Sensitivity analysis of the operating and technical specifications of a solar chimney power plant. J. Solar Energy Eng. 129, 171–178.

Pretorius, J.P., Kröger, D.G., 2008. Thermoeconomic optimization of a solar chimney power plant. J. Solar Energy Eng. 130, 021015-1–021015-9.

Sangi, R., Amidpour, M., Hosseinizadeh, B., 2011. Modeling and numerical simulation of solar chimney power plants. Solar Energy 85, 829–838.

Schlaich, J., Bergermann, R., Schiel, W., Weinrebe, G., 2004. Sustainable electricity generation with solar updraft towers. Struct. Eng. Int. 14, 225–229.

von Backström, T.W., 2003. Calculation of pressure and density in solar power plant chimneys. J. Solar Energy Eng. 125, 127–129.

Zhou, X., Yang, J., Xiao, B., Hou, G., 2007. Simulation of a pilot solar chimney thermal power generating equipment. Renew. Energy 32, 1637–1644.

Zhou, X., Bernardes, M.A.d.S., Ochieng, R.M., 2012. Influence of atmospheric cross flow on solar updraft tower inflow. Energy 42, 393–400.

Zhou, X., Xu, Y., Yuan, S., Chen, R., Song, B., 2014. Pressure and power potential of sloped-collector solar updraft tower power plant. Int. J. Heat Mass Transfer 75, 450–461.